Band termination and second backbending in ^{50}Cr

S. M. Lenzi,[1] C. A. Ur,[1,*] D. R. Napoli,[2] M. A. Nagarajan,[2] D. Bazzacco,[1] D. M. Brink,[3] M. A. Cardona,[4] G. de Angelis,[2] M. De Poli,[2] A. Gadea,[2] D. Hojman,[4] S. Lunardi,[1] N. H. Medina,[1,†] and C. Rossi Alvarez[1]

[1]*Dipartimento di Fisica and INFN, Padova, Italy*

[2]*Laboratori Nazionali di Legnaro, INFN, Legnaro, Italy*

[3]*Dipartimento di Fisica and INFN, Trento, Italy*

[4]*Departamento de Física, CNEA, Buenos Aires, Argentina*

(Received 8 May 1997)

High-spin states in ^{50}Cr have been investigated with the reaction ^{24}Mg(^{32}S,$\alpha 2p$) at 130 MeV bombarding energy, using the 4π GASP γ-ray array plus the 4π charged-particle detector ISIS. The level scheme has been extended up to the 18^+ state at 17.954 MeV excitation energy. Several high-spin states which deexcite by emitting high energy γ-rays have been identified. A second backbending is observed at $I=18\hbar$, well above the 14^+ state which exhausts the total spin available in a pure $(f_{7/2})^{10}$ configuration. [S0556-2813(97)03109-9]

PACS number(s): 23.20.Lv, 23.20.En, 25.70.Gh, 27.40.+z

I. INTRODUCTION

The spectroscopy of $1f_{7/2}$ nuclei provides a good test for shell model calculations and associated effective interactions. A great amount of work, from both theoretical and experimental sides, was done about twenty years ago in this mass region. Strong deformation was attributed to nuclei near the middle of the shell, i.e., ^{48}Cr and neighboring nuclei. However, due to experimental difficulties, only relatively low-spin states were identified. In addition, shell model (SM) calculations in this region have been mainly restricted to the $f_{7/2}$ shell or to few particle excitations in the fp shell. It is only recently that the new refinements of the theoretical methods, together with the advent of highly efficient detector arrays, have opened the possibility of studying these relatively light nuclei at high spins where the interplay between single particle and collective degrees of freedom is expected to be clearly exhibited.

In the past few years, shell model calculations in the full fp shell, which reproduce with good accuracy the new experimental data, have become available in this mass region [1]. The nucleus ^{48}Cr, with four protons and four neutrons outside the doubly closed shell nucleus ^{40}Ca, has the maximum number of particles to develop deformation in the $f_{7/2}$ shell and displays, in fact, a rotational-like ground state band. This band has been recently extended to higher spins [2,3] and the shell model predictions [4] are in very good agreement with the observed level scheme. A complementary comparison with deformed mean field approaches, such as the cranked Hartree Fock Bogoliubov (CHFB) method, allows for a better understanding of the underlying dynamical properties. Aside from the case of ^{48}Cr, other neighboring nuclei display collective behavior in this mass region. In a recent paper [5], Martínez-Pinedo and co-workers have performed theoretical studies for ^{50}Cr in the framework of the full fp spherical shell model and of the CHFB approach. They have reproduced very well the yrast energies up to spin $I=12\hbar$ [6], which includes the backbending region around $I=10\hbar$, and have predicted a second backbending at $I=18\hbar$ in this nucleus. Experimentally, however, no evidence of this latter phenomenon has been reported so far in ^{50}Cr.

Backbending phenomena, as well as changes of shape, can be understood in terms of the dynamical evolution of the interactions with increasing excitation energy and angular momentum. In explaining these properties, however, one has to be careful not to extrapolate directly the arguments usually applied to heavier nuclei. In $f_{7/2}$-shell nuclei, neutron-proton correlations play a crucial role because valence nucleons are filling the same shell. Therefore, an interpretation of the backbending based on the alignment of like-nucleon pairs, which holds for higher masses where neutrons and protons align independently, has to be revised in this mass region. For $N=Z$ nuclei in a single-j shell, cranked deformed shell-model calculations which include $T=0$ and $T=1$ pairing correlations, predict the simultaneous alignment of two-proton and two-neutron pairs [7]. This actually seems to be the case of ^{48}Cr [8]. The same model predicts, furthermore, that ^{50}Cr, with four protons and two neutron holes in the $f_{7/2}$ shell, should become soft against triaxiality with increasing rotational frequency [9].

The rotational properties of the $f_{7/2}$ nuclei are also affected by the underlying microscopic structure since the valence nucleons can align fully along the rotational axis creating band-terminating states. A fingerprint of the band-termination process in this mass region could be the smooth decrease of the moment of inertia as the nucleus approaches the upper limit of spin available in the single-j shell. Yet, another indication could be the occurrence of high energy transitions connecting the band-termination state with states of higher angular momentum [10].

High-spin spectroscopy is not an easy task in this mass region for the following reasons: (a) the angular momentum of the compound nucleus in a fusion-evaporation reaction is restricted because of the light masses of the reaction partners, (b) the high velocity of the light recoils together with the effects on the kinematics due to the evaporation of charged

*On leave from National Institute of Physics and Nuclear Engineering, Bucharest, Romania.

†Present address: Universidade de São Paulo, Brazil.

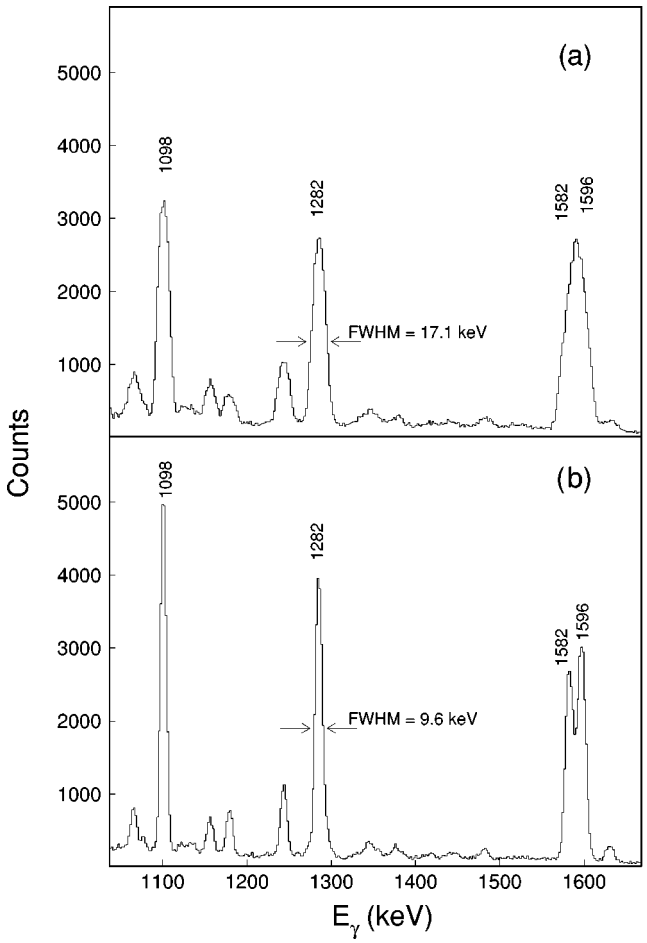

FIG. 1. Projection spectra of the γ-γ-γ coincidence cubes conditioned with $\alpha 2p$ particles (a) without and (b) with the kinematical Doppler correction according to the detection geometry of the charged particles. It is emphasized the energy resolution improvement for the 1.282 MeV γ-ray transition of about 44%.

particles (i.e., α particles), considerably increases the width of the peaks, (c) as the spin increases, the energy of the transitions become very high, which implies poor resolution and detection efficiency, and (d) the number of competing channels with evaporation of charged particles becomes very large. Despite these limitations, the possibility of simultaneously detecting charged particles and gamma rays with high efficiency, that has become available with the new 4π γ-ray spectrometers, provides a powerful technique for selecting the individual channels and for reconstructing the kinematics, allowing for an improvement in energy resolution.

In this work we present new results on the high-spin properties of ^{50}Cr. Experimental and data analysis details, together with the adopted level scheme, are described in Sec. II. The discussion of the results is presented in Sec. III. Conclusions are given in Sec. IV.

II. MEASUREMENTS AND RESULTS

A. Experimental and data analysis details

We have populated the nucleus ^{50}Cr with the reaction ^{24}Mg(^{32}S,$\alpha 2p$) at 130 MeV bombarding energy. The beam was provided by the Tandem XTU accelerator of the Legnaro National Laboratory. A self–supporting ^{24}Mg target with a 400 μg/cm^2 thickness was used. The experimental setup consisted of the 4π GASP γ-ray array [11], which is composed of 40 Compton-suppressed large volume HPGe detectors and a multiplicity filter of 80 BGO crystals, plus the 4π charged-particle detector ISIS consisting of 40 (ΔE,E) Si telescopes. Events were collected when at least two Ge detectors and two elements of the multiplicity filter fired in coincidence. Energy calibration of the spectra and gain matching between the different Ge detectors have been performed using sources of ^{56}Co, ^{133}Ba, and ^{152}Eu.

After the unfolding, a total of 570 million double events and 65 million triple events were available for the offline analysis. Since high energy transitions were expected at high spin in ^{50}Cr, we recorded on tape γ-ray energies up to 8 MeV. The determination of the direction of the emitting residual nucleus has been possible on an event-by-event basis by identifying the emission angle of the charged particles in the ISIS detector, thus allowing for a precise Doppler shift correction. This led to an improvement in the gamma-ray energy resolution of $\sim$ 40% at 1.3 MeV, as can be seen in Fig. 1.

The quality of the γ-γ coincidence spectra used in our analysis is illustrated in Fig. 2 which shows a γ-ray spectrum with gates set on all transitions connecting yrast states of ^{50}Cr. Gamma rays up to 5.5 MeV can be clearly identified.

The directional correlations of oriented states (DCO ratios [12]) have been estimated according to the relation:

$$R_{\mathrm{DCO}}=\frac{I_{\gamma_1}(\text{at } \theta_1 \text{ gated by } \gamma_2 \text{ at } \theta_2)}{I_{\gamma_1}(\text{at } \theta_2 \text{ gated by } \gamma_2 \text{ at } \theta_1)}, \tag{1}$$

where γ_1 is the gamma ray under investigation while γ_2 is the gamma ray of known multipolarity. The DCO ratios have been extracted from a γ-γ matrix containing the correlations between gamma rays detected in the 12 detectors at 34° and 146° (θ_1) on one side, and those detected in the 8 detectors placed at 90° (θ_2) on the other side. In the GASP geometry, if one gates on a stretched quadrupole transition, the theoretical DCO ratios are $\sim$ 1 for stretched quadrupole transitions and $\sim$ 0.5 for pure dipole ones. If, on the contrary, gates are set on pure dipole transitions, the expected DCO ratios for quadrupole and dipole transitions are $\sim$ 2 and $\sim$ 1, respectively.

In order to take advantage of the high statistics available from the GASP array we also made use of the γ-ray angular distribution from oriented nuclei (ADO ratios [13]). In large gamma arrays, where detectors are placed at many different angles, by summing up all the angles, the angular correlation between two gammas disappears. Consequently, the intensity of a particular transition in a spectrum obtained by setting a gate on the matrix axis with all the angles, does not depend on the multipole character of the gating transition, but follows the regular angular distribution law as a function of the observation angle. The ADO ratios are defined as

$$R_{\mathrm{ADO}}=\frac{I_{\gamma_1}(\text{at } \theta_1 \text{ gated by } \gamma_2)}{I_{\gamma_1}(\text{at } \theta_2 \text{ gated by } \gamma_2)} \tag{2}$$

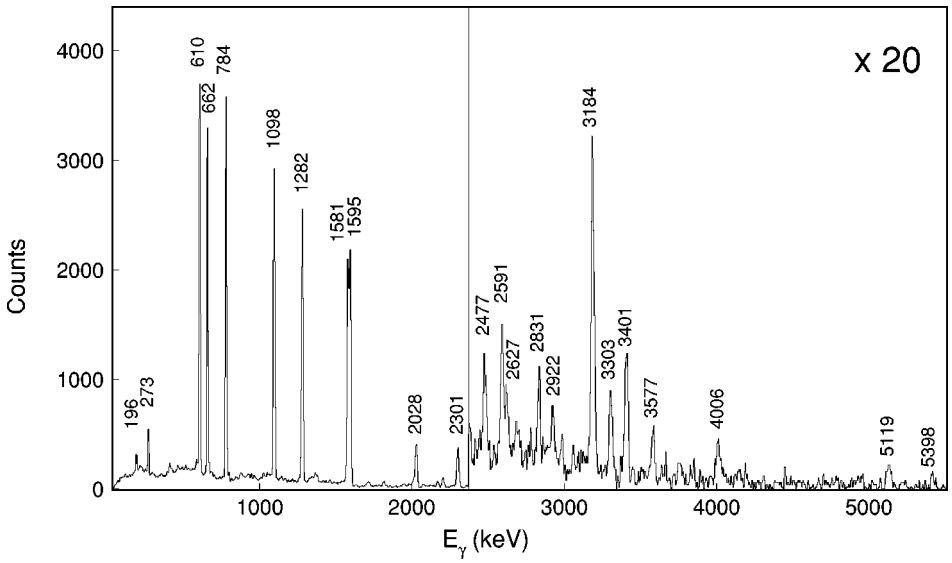

FIG. 2. Coincidence γ-ray spectrum showing the transitions in ^{50}Cr. The spectrum was created by summing up doubly-gated spectra on all the transitions in the yrast band obtained from a γ-γ-γ coincidence cube conditioned with $\alpha 2p$ particles. Transitions are labeled by their energy in keV.

These values were extracted from two γ-γ coincidence matrices containing: one, the detectors at 34° and 146° (θ_1) versus the sum of all the detectors, and the other, the detectors at 90° (θ_2) versus all the detectors. The gate on the γ_2 transition is set on the axis where all the detectors are added together. The intensities of the γ rays have been corrected for the detection efficiency of the corresponding ring of detectors. Typical ADO ratios for stretched quadrupole transitions are $\sim$1.25 and for stretched pure dipole transitions $\sim$0.7. In Fig. 3 ADO ratios are plotted for several γ-ray transitions in ^{50}Cr. The γ-ray energies, relative intensities, DCO and ADO ratios are listed in Table I together with the deduced spin assignments.

B. The level scheme

The level scheme of ^{50}Cr deduced from the present study is shown in Fig. 4. The assignment of new transitions and their placement in the level scheme were based on the coincidence with charged particles, γ-γ coincidence relationships and relative intensities. Spin assignments were based on DCO and ADO analysis results and on the decay patterns.

The parity of the levels has been established assuming that, when gating on a $\Delta I=2$ stretched quadrupole transition, the strong transitions with DCO ratios $\sim$ 1 have $E2$ character and the transitions with DCO ratios definitely different from 1 and 0.5 are of mixed multipolarity ($M1+E2$ character).

At low spin, a single band structure is found. Above the 12_1^+ level, the scheme becomes much more complex and displays a peculiar ''treelike'' pattern with several high-energy transitions (up to 5.4 MeV).

We confirm all the known yrast states up to the 12_1^+ at 7.612 MeV [6]. Below this level, only one new state has been identified, namely the second 10^+ state at 6.753 MeV. Its spin-parity assignment is straightforward from the DCO and ADO ratios of the transitions (2009.3, 414.5, and 196.3 keV) which connect the 10_2^+ state with the known levels in ^{50}Cr. A very weak $E2$ ($\sim$ 3% of relative intensity) crossover transition of 1.272 MeV connecting the 12_1^+ and the 10_1^+ state has been also observed.

The 12_1^+ level is fed by several strong $M1$ transitions, apart from the 2.301 MeV and 4.928 MeV transitions from the 14_1^+ and 14_2^+ levels, respectively, which are identified as stretched quadrupole. A transition of particularly high energy (5.119 MeV) defines the yrast 16^+ state at 15.032 MeV. This state is fed by a stretched quadrupole transition of 2.922 MeV which establishes the 18^+ state at 17.954 MeV, giving the evidence for a second backbending in the yrast band of ^{50}Cr.

Recent experimental studies by Cameron and co-workers have also investigated the structure of ^{50}Cr at high spin [14].

III. DISCUSSION

Near the ground state, ^{50}Cr behaves as an imperfect prolate rotor. This quadrupole collectivity is well reproduced by shell model calculations of Martínez-Pinedo and co-workers [5]: the wave functions for the first five yrast states have a large $f_{7/2}$ component but also the $p_{3/2}$ shell is appreciably occupied; the calculated spectroscopic quadrupole moments

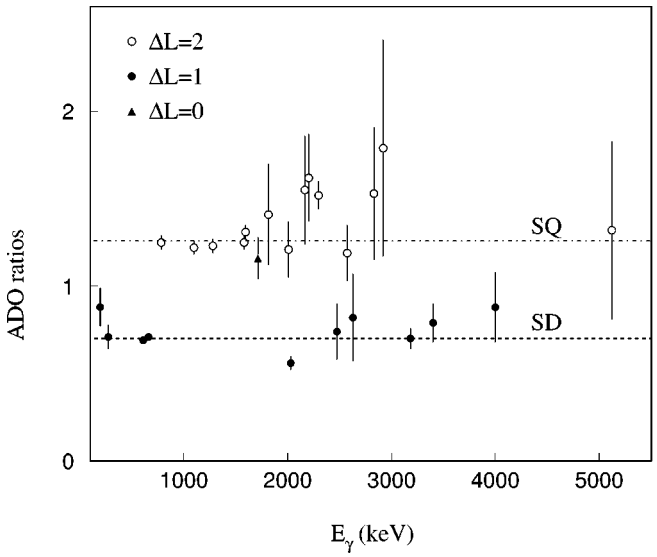

FIG. 3. ADO ratios of the most intense transitions in ^{50}Cr. Typical behaviour of the stretched quadrupole (SQ) and pure stretched dipole (SD) transitions, respectively, are indicated by dashed lines (see text for explanations).

TABLE I. Relative intensities, DCO, ADO, and tentative spin assignments for ^{50}Cr.

E_γ (keV)	Intensity [a]	DCO ratios [b]	ADO ratios	Assignment [c]
196.3	2.5(8)	1.06(13) *D*	0.88(11)	$11_1^+ \rightarrow 10_2^+$
273.3	9.2		0.71(7)	$14_1^+ \rightarrow 13_1^+$
414.5	1.5(5)	0.96(19) *Q*		$10_2^+ \rightarrow 10_1^+$
610.3	73.4	0.59(9) *Q*	0.69(1)	$11_1^+ \rightarrow 10_1^+$
662.4	69.1	1.03(12) *D*	0.71(1)	$12_1^+ \rightarrow 11_1^+$
783.6	100.0	1.11(16) *Q*		$2_1^+ \rightarrow 0_1^+$
1097.9	100.0	1.06(12) *Q*		$4_1^+ \rightarrow 2_1^+$
1272	3.0(10)			$12_1^+ \rightarrow 10_1^+$
1282.3	100.0	1.11(17) *Q*		$6_1^+ \rightarrow 4_1^+$
1580.5	100.0	1.97(25) *D*	1.25(4)	$8_1^+ \rightarrow 6_1^+$
1593.6	7.0(10)			$(15_1) \rightarrow 13_2^+$
1595.2	82.9	1.86(24) *D*	1.31(4)	$10_1^+ \rightarrow 8_1^+$
1713.8	1.7(5)		1.16(12)	$12_2^+ \rightarrow 12_1^+$
1815.5	3.2(5)		1.41(29)	$16_1^+ \rightarrow 15_2^+$
2009.3	8.2(10)	1.03(18) *Q*	1.21(16)	$10_2^+ \rightarrow 8_1^+$
2028.1	18.6	0.69(12) *D*	0.56(4)	$13_1^+ \rightarrow 12_1^+$
2168.1	1.7(5)		1.55(31)	$16_2^+ \rightarrow 14_3^+$
2204.2	5.6		1.62(25)	$15_2^+ \rightarrow 13_1^+$
2300.9	20.9	2.00(24) *D*	1.52(8)	$14_1^+ \rightarrow 12_1^+$
2476.9	2.8(6)	0.57(10) *Q*	0.74(16)	$15_1^+ \rightarrow 14_1^+$
2492.1	1.0(5)			$16_1^+ \rightarrow 14_2^+$
2572.6	2.0(7)		1.19(16)	$12_2^+ \rightarrow 10_2^+$
2590.5	4.5(10)			$16_2^+ \rightarrow 15_2^+$
2627.1	1.8(5)		0.82(25)	$14_3^+ \rightarrow 13_3^+$
2830.9	3.4		1.53(38)	$17_1^+ \rightarrow 15_2^+$
2921.6	2.0(5)		1.79(62)	$18_1^+ \rightarrow 16_1^+$
2987	<1.0			$12_2^+ \rightarrow 10_1^+$
3183.9	11.3	0.75(12) *D*	0.70(6)	$13_2^+ \rightarrow 12_1^+$
3303.3	3.0	0.48(8) *Q*		$15_2^+ \rightarrow 14_1^+$
3400.5	8.4	0.76(13) *Q*	0.79(11)	$13_3^+ \rightarrow 12_1^+$
3577.1	3.0(5)			$15_2^+ \rightarrow 13_1^+$
3748.2	1.2(5)			$(17_2) \rightarrow 15_4^+$
4005.8	3.3(4)	0.38(6) *Q*	0.88(20)	$15_4^+ \rightarrow 14_1^+$
4927.9	6.0			$14_2^+ \rightarrow 12_1^+$
5119.1	11.0		1.32(51)	$16_1^+ \rightarrow 14_1^+$
5398.2	5.6			$(16_3) \rightarrow 15_1^+$

[a]Errors higher than 10% are specified. For transition energies higher than 4 MeV errors of the intensities could be even of the order of 50%.

[b]The letters after the ratio values have the following meaning: *D* when the gate was set on a dipole transition and *Q* when the gate was set on a quadrupole transition.

[c]The indices are specifying the ordering in energy of the states with the same spin.

are negative and consistent with a rather constant intrinsic quadrupole moment. The deformation parameters calculated by those authors in the framework of the CHFB method are $\beta \simeq 0.22$ and $\gamma \simeq 0$ for the yrast states up to $I = 8\hbar$.

In a recent paper, Zamick, Fayache, and Zheng [15] have performed truncated shell model calculations for ^{50}Cr using the FPD6 and the KB3 interactions. Both interactions agree in predicting negative quadrupole moments up to $I = 8\hbar$, but give different values for the two $I = 10\hbar$ levels. When using the FPD6 interaction, the quadrupole moments of the two 10^+ states take different signs, the 10_2^+ state has a negative value, while the 10_1^+ becomes positive. The calculated $B(E2{:}10_2^+ \rightarrow 8^+)$ is 140 e^2 fm^4 and the $B(E2{:}10_1^+ \rightarrow 8^+)$ is 28.7 e^2 fm^4. On this basis, the authors [15] pointed out that the 10_2^+ state should be considered as a member of the ground state band. When these calculations are performed with the KB3 interaction, however, positive quadrupole moments and comparable $B(E2)$'s are obtained for both 10^+ states [15,16]. These latter results agree with those obtained in Ref. [5] with a full fp shell model calculation using the KB3 interaction. Furthermore, the branching ratios predicted in Ref. [5] [using the theoretical $B(E2)$'s and the experimental energies] for the decay of both 10^+ states are in very good agreement with those observed experimentally. This seems to confirm that both 10^+ states have positive quadrupole moments which indicates that there is a sudden change in the intrinsic configuration between $I = 8\hbar$ and $I = 10\hbar$. The measurement of the lifetimes will put more light on this point.

The first backbending in ^{50}Cr observed at the 10_1^+ state can be related to the change of sign in the quadrupole moments. Above $I = 10\hbar$, positive quadrupole moments are also predicted for the yrast states up to spin $I = 14\hbar$. On the basis of these considerations, the first backbending in ^{50}Cr has been interpreted as due to a band crossing: the second band (from 10_1^+ to 14_1^+) being that of an oblate rotor [5] or a high-K band [16].

Another possible interpretation relies on the change of deformation induced by the reduced number of valence rotons and neutrons. As pointed out in Sec. I, ^{50}Cr is predicted to become soft against γ deformation at high rotational frequency; the four protons drive the nucleus towards prolate deformation, while the two neutron holes drive it into the oblate direction [9]. From the experimental side, a sudden loss of quadrupole collectivity above spin $I = 10\hbar$ is observed in the level scheme of ^{50}Cr (see Fig. 4 and Table I). Two strong dipole γ rays from the 11^+ and 12^+ states are seen, while a very weak crossover stretched $E2$ transition connects the 12^+ and the 10_1^+ levels. The experimental branching ratios for the $12^+ \rightarrow 10_1^+$ (4%) and $12^+ \rightarrow 11^+$ (96%) are in very good agreement with the SM predictions (calculated by using the experimental energies). Furthermore, both SM and CHFB calculations in Ref. [5] show a rapid decrease of the $p_{3/2}$ contribution to the nucleus wave function above $I = 10\hbar$, which causes a loss of quadrupole coherence. This is consistent with the fact that the mechanism of generating angular momentum by aligning the valence particle spins along the rotational axis in a high-j shell, becomes energetically favored at high frequency. This interplay between single article and collective motion is illustrated in Fig. 5, where we plot the excitation energy, normalized to that of a rigid rotor, as a function of the angular momentum. During this aligning process, the nucleus undergoes changes of shape, from collective prolate to (eventually) triaxial and noncollective oblate.

At $I = 14\hbar$ the nucleus reaches the maximum angular momentum that can be constructed with 4 protons and

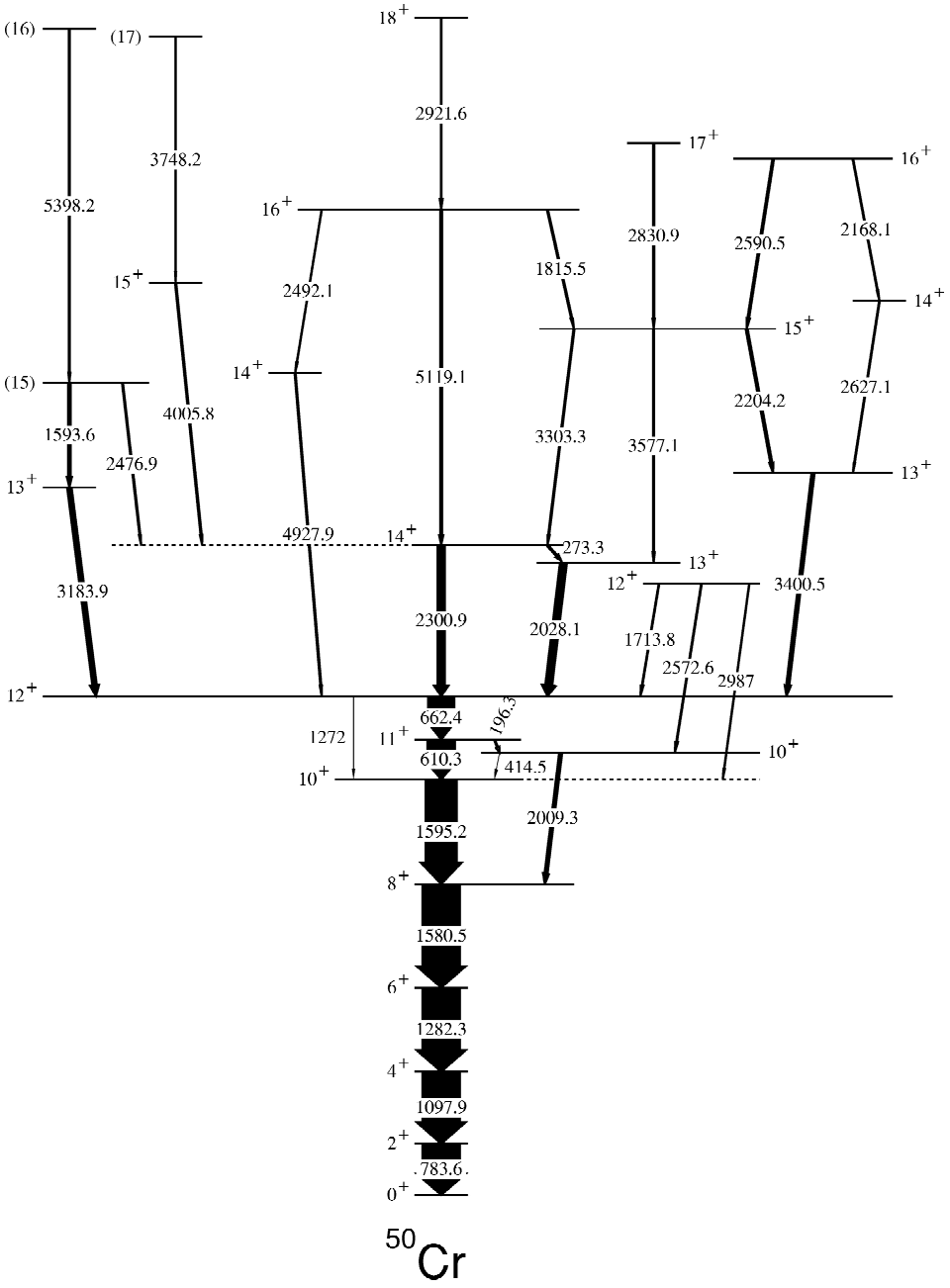

FIG. 4. Level scheme of ^{50}Cr obtained in this experiment. Energies of the γ-ray transitions are given in keV. The widths of the arrows are proportional to the measured intensities (Table I).

6 neutrons in the single $f_{7/2}$ shell. In Ref. [5], shell model, as well as CHFB calculations give a description of the 14^+ state wave function as mainly $(f_{7/2})^{10}$ configuration. The calculated branching ratios for the decay of this state are in good agreement with those observed experimentally. With the spins fully aligned with the rotational axis, the valence particles rotate in orbits near the equator of the core, making an oblate noncollective band-terminating state.

To generate higher spins, valence nucleons have to be promoted to high lying orbits. This process gives rise to the high-energy transition that connects the 16^+_1 and 14^+_1 states and, according to shell model calculations [5] this should be due to neutron excitations into the $f_{5/2}$ shell, which lies about 6 MeV above the $f_{7/2}$. These calculations predict also that the most intense decay from the 16^+ state should go to the 14^+_2 state. Experimentally, however, the most intense transition observed to depopulate the 16^+ goes to the first 14^+_1. The nucleus prefers to deexcite along the yrast line.

The highest spin state observed in this experiment is 18^+, which decays to the 16^+_1 by a stretched quadrupole γ ray of 2.922 MeV. A second backbending is apparent at $I=18\hbar$. The next level with spin $I=20\hbar$ is predicted to lay 4.8 MeV above the 18^+, but has not been seen in this experiment. The structure of the 18^+, as well as the 16^+, are calculated as almost purely $\pi(f_{7/2})^4\ \nu(f_{7/2})^5 f_{5/2}$ configuration [5]. At $I=20\hbar$, a further neutron excitation to the $p_{3/2}$ shell occurs. The probability predicted for the transition $20^+\rightarrow 18^+$ is very low: the $B(E2,20^+\rightarrow 18^+_1)$ is 0.24 e^2 fm^4. The second backbending in ^{50}Cr is thus interpreted as due to single particle effects. The observation of the 20^+ and higher levels awaits further experiments to be performed with the new generation γ-ray arrays.

The stretched quadrupole sequence of γ-ray transitions for the yrast band of ^{50}Cr is plotted in Fig. 6 versus the

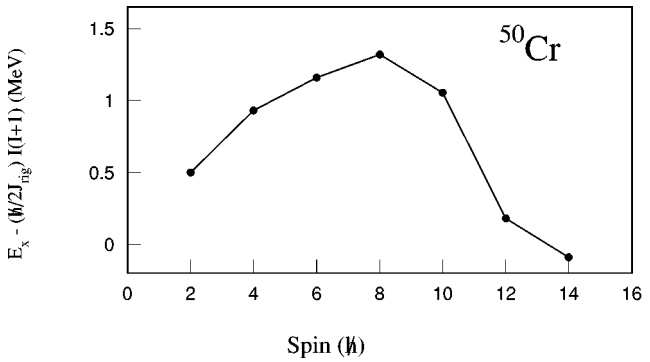

FIG. 5. Excitation energy, minus an average rigid rotor contribution, vs the total spin up to the band-terminating state at $I=14\hbar$.

angular momentum I as deduced from this work and compared with the full fp shell model predictions [5]. The agreement between theory and experiment for the $E2$ transitions is impressive. Furthermore, there is also good agreement for most of the nonyrast state energies [17] and for the yrast branching ratios.

IV. CONCLUSIONS

The level scheme of ^{50}Cr has been extended above band termination using the 4π GASP γ-ray array combined with the charged-particle detector array ISIS. The very good efficiency of both spectrometers has allowed for the observation of the high spin structure, characterized by high energy γ-ray transitions. The nucleus ^{50}Cr shows quadrupole collectivity at low and intermediate spins. With increasing rotational frequency, several effects due to the interplay between single particle and collective properties have been observed. The first backbending is interpreted as a consequence of a change of shape from collective prolate to triaxial or noncollective oblate, due to the gradual alignment of the individual valence particles in the $f_{7/2}$ shell. The number of valence protons and neutrons of ^{50}Cr is sufficiently big to produce collective motion at low and intermediate spins but small enough to give rise to band terminating states at high spin. Two high energy $E2$ transitions have been observed above the maximum spin ($I=14\hbar$) that can be constructed with 10 particles in the $f_{7/2}$ shell, which define the 16^+ and 18^+ yrast states. The large energy gap between the 16^+_1 and 14^+_1 states is interpreted as a fingerprint of band termination in this mass region. It is consistent with a change of configuration in which particles are excited to the high lying $f_{5/2}$ shell [5]. A second backbending is apparent in the highest spin region, in which the nucleus has lost most of its quadrupole coherence.

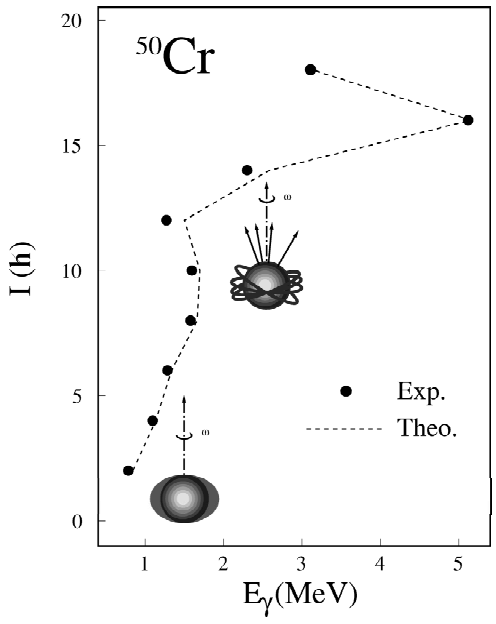

FIG. 6. Experimental and shell model stretched quadrupole yrast transitions of ^{50}Cr. Theoretical values are taken from Ref. [5].

As in the case of ^{48}Cr, the nucleus ^{50}Cr is a good testing ground to compare two different theoretical descriptions: the spherical shell model, which provides an exact calculation in the laboratory frame, and the cranked Hartree-Fock-Bogoliubov method, which allows a description in terms of the intrinsic state that gives rise to the collective rotational ground-state band [5]. A very good agreement between these calculations and the data reported in this work for ^{50}Cr is found.

Above spin $I=18\hbar$, ^{50}Cr is predicted to develop triaxial deformation [5]. The experimental study of these *very high spin* states will become soon feasible with the advent of the new generation of multidetector γ-ray facilities. A further test of the theoretical descriptions awaits the measurement of lifetimes of the high-spin states in this mass region.

ACKNOWLEDGMENTS

We thank B. F. Bayman, F. Brandolini, G. Martínez-Pinedo, A. Poves, I. Ragnarsson, and A. Vitturi for fruitful discussions. A.G. was supported by the EC under Contract No. ERBCHBGCT940713.

[1] E. Caurier, A.P. Zuker, A. Poves, and G. Martinez-Pinedo, Phys. Rev. C **50**, 225 (1994).

[2] S.M. Lenzi, D.R. Napoli, A. Gadea, M.A. Cardona, D. Hojman, M.A. Nagarajan, C. Rossi Alvarez, N.H. Medina, G. de Angelis, D. Bazzacco, M.E. Debray, M. De Poli, S. Lunardi, and D. de Acuña, Z. Phys. A **354**, 117 (1996).

[3] J.A. Cameron, J. Jonkman, C.E. Svensson, M. Gupta, G. Hackman, D. Hyde, S.M. Mullins, J.L. Rodriguez, J.C. Waddington, A. Galindo-Uribarri, H.R. Andrews, G.C. Ball, V.P. Janzen, D.C. Radford, D. Ward, T.E. Drake, M. Cromaz, J. DeGraaf, and G. Zwartz, Phys. Lett. B **387**, 266 (1996).

[4] E. Caurier, J.L. Egido, G. Martinez-Pinedo, A. Poves, J. Retamosa, L.M. Robledo, and A.P. Zuker, Phys. Rev. Lett. **75**, 2466 (1995).

[5] G. Martínez-Pinedo, A. Poves, L.M. Robledo, E. Caurier, F. Nowacki, J. Retamosa, and A. Zuker, Phys. Rev. C **54**, R2150 (1996).
[6] T.W. Burrows, Nucl. Data Sheets **75**, 1 (1995).
[7] J.A. Sheikh, N. Rowley, and M.A. Nagarajan, Phys. Lett. B **240**, 11 (1990).
[8] J.A. Sheikh, M.A. Nagarajan, and S.M. Lenzi (unpublished).
[9] S. Frauendorf, J.A. Sheikh, and N. Rowley, Phys. Rev. C **50**, 196 (1994).
[10] I. Ragnarsson, V.P. Janzen, D.B. Fossan, N.C. Schmeing, and R. Wadsworth, Phys. Rev. Lett. **74**, 3935 (1995).
[11] D. Bazzacco, Proceedings of the International Conference on Nuclear Structure at High Angular Momentum, Ottawa, 1992 [Report No. AECL 10613 (unpublished)], Vol. II, p. 376.
[12] K.S. Krane, R.M. Steffen, and R.M. Wheeler, Nucl. Data Tables **11**, 351 (1973).
[13] M. Piiparinen, A. Ataç, J. Blomqvist, G.B. Hagemann, B. Herskind, R. Julin, S. Juutinen, A. Lampinen, J. Nyberg, G. Sletten, P. Tikkanen, S. Tormanen, A. Virtanen, and R. Wyss, Nucl. Phys. **A605**, 191 (1996).
[14] J.A. Cameron *et al.* (unpublished).
[15] L. Zamick, M. Fayache, and D.C. Zheng, Phys. Rev. C **53**, 188 (1996).
[16] L. Zamick and D.C. Zheng, Phys. Rev. C **54**, 956 (1996).
[17] G. Martínez-Pinedo (private communication).